COMMUNICATIONS IN COMPUTATIONAL PHYSICS
Vol. **6**, No. 1, pp. 162-184

Commun. Comput. Phys.
July 2009

Multiscale Modeling and Simulations of Flows in Naturally Fractured Karst Reservoirs†

Peter Popov[1,*], Yalchin Efendiev[2] and Guan Qin[1]

[1] *Institute for Scientific Computation, Texas A&M University, College Station, TX 77843.*
[2] *Department of Mathematics, Texas A&M University, College Station, TX 77843.*

Received 23 January 2008; Accepted (in revised version) 8 August 2008

Available online 18 November 2008

Abstract. Modeling and numerical simulations of fractured, vuggy, porus media is a challenging problem which occurs frequently in reservoir engineering. The problem is especially relevant in flow simulations of karst reservoirs where vugs and caves are embedded in a porous rock and are connected via fracture networks at multiple scales. In this paper we propose a unified approach to this problem by using the Stokes-Brinkman equations at the fine scale. These equations are capable of representing porous media such as rock as well as free flow regions (fractures, vugs, caves) in a single system of equations. We then consider upscaling these equations to a coarser scale. The cell problems, needed to compute coarse-scale permeability of Representative Element of Volume (REV) are discussed. A mixed finite element method is then used to solve the Stokes-Brinkman equation at the fine scale for a number of flow problems, representative for different types of vuggy reservoirs. Upscaling is also performed by numerical solutions of Stokes-Brinkman cell problems in selected REVs. Both isolated vugs in porous matrix as well as vugs connected by fracture networks are analyzed by comparing fine-scale and coarse-scale flow fields. Several different types of fracture networks, representative of short- and long-range fractures are studied numerically. It is also shown that the Stokes-Brinkman equations can naturally be used to model additional physical effects pertaining to vugular media such as partial fracture with fill-in by some material and/or fluids with suspended solid particles.

AMS subject classifications: 35B27, 35Q30, 6S05
Key words: Homogenization, Stokes equation, Brinkman equation, porous media.

1 Introduction

Naturally fractured karst reservoirs presents multiple challenges for numerical simulations of various fluid flow problems. Such reservoirs are characterized by the presence

†Dedicated to Richard Ewing, whose untimely death we mourn.
*Corresponding author. *Email addresses:* ppopov@tamu.edu (P. Popov), efendiev@math.tamu.edu (Y. Efendiev), guan.qin@tamu.edu (G. Qin)

of fractures, vugs and caves at multiple scales, as shown in Fig. 1. The media can be described, at each individual scale, as an ensemble of porous media with well defined properties (porosity and permeability), and a free flow region where the fluid (oil, water, gas) meets no resistance form the surrounding rock [13].

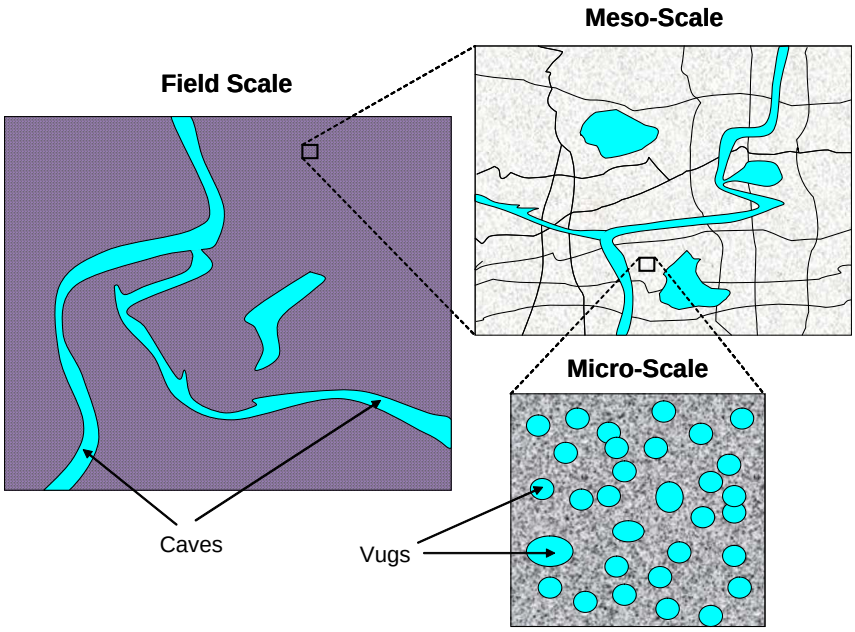

Figure 1: Conceptual model of a vuggy, fractured reservoir at multiple scales.

The main difficulty in numerical simulations in such reservoirs is the co-existence of porous and free flow regions, typically at several scales. The presence of individual voids such as vugs and caves in a surrounding porous media can significantly alter the effective permeability of the media. Furthermore, fractures and long range caves can form various types of connected networks which change the effective permeability of the media by orders of magnitudes. An additional factor which complicates the numerical modeling of such systems is the lack of precise knowledge on the exact position of the interface between the porous media (rock) and the and vugs/caves. Finally, the effects of cave/fracture fill in by loose material (sand, mud, gravel, etc), the presence of damage at the interface between porous media and vugs/caves and the roughness of fractures can play very important role in the overall response of the reservoir.

The modeling of fractured, vuggy media is traditionally done by two different approaches. The first approach, which has usually been used for vuggy media, is to use the coupled Stokes-Darcy equations [2,4,13–17,20,26,28,29]. The porous regions is modeled by the Darcy equation [8,29], while the Stokes equation (c.f., e.g., [22]) is used in the free flow region. At the interface between the two, various types of interface conditions are postulated [4,20,26,29]. All of these interface conditions require continuity of mass and

momentum across the interface. The difference comes when the tangential component of the velocity at the interface is treated. Each one of them proposes a different jump condition for the tangential velocity and/or stresses, related in some way to the fluid stress. The selection of jump condition is subject to the fine structure of the interface and the flow type and regime (c.f., e.g., [19], and the references therein). Furthermore, these jump conditions introduce additional media parameters that need to be determined. These parameters can be obtained either experimentally or computationally.

There are several aspects of the coupled Darcy-Stokes approach which make its application to vuggy reservoirs complicated. First, a very detailed knowledge is required both in the exact location and the fine-scale structure of the porous/fluid interface. Such precise information is hard to deduce from subsurface geological data. Secondly, there is need to obtain, numerically or experimentally, values for parameters related to the interface conditions. Numerical determination is viable for engineered media, such as oil filters in the automotive industry, where the fine-scale porous geometry is known, either by design, or can be obtained relatively easily, for example by 3D tomography. The experimental approach is more appropriate for subsurface formations, however, there are many difficulties associated with it. Finally, the free flow region which represents caves/vugs and fractures must be free of any obstacles such as loose fill-in material, and the fluid must also be free of any particle suspensions which are moving with it.

An alternative way of modeling vuggy media is to use the Stokes-Brinkman equations [1, 5, 13, 18, 19, 21, 23, 24]. These equations provide a unified approach in the sense that a single equation with variable coefficients is used for both porous and free-flow region. Stokes-Brinkman equations can be reduced to Stokes or Darcy equations by appropriate choice of the parameters. Since the different media types are distinguished by selecting the coefficients of the PDE, there is usually no need to formulate specific interface conditions. This is especially helpful in reservoir and groundwater flow, where the porous domain has a complicated topology. The numerical treatment of Stokes-Brinkman equation is simpler, due the lack of special interface conditions. Also, due to uncertainties associated with interface locations between vugs and the rock matrix, Stokes-Brinkman equations introduce a somewhat coarse model that does not require precise interface locations and avoid local grid refinement issues that are needed near the interfaces. Finally the Stokes-Brinkman equations provide a model that can be continuously varied from a Darcy dominated flow to a Stokes dominated flow, a feature which allows is to simulate effectively partially filled fractures or solid particles suspended in the fluid.

In this paper we consider the Stokes-Brinkman equation as a fine-scale model for flows in vuggy, fractured karst reservoirs. The mathematical model is presented in Section 2. The upscaling of this equation is summarized in Section 2.3. Next, a mixed finite element method (Section 3.1) is used to solve the Stokes-Brinkman equation for a number of flow problems, representative for fractured, vuggy reservoirs. We have analyzed both isolated vugs in porous matrix (Sections 3.2 and 3.3) as well as vugs connected by fracture networks (Section 4). Different types of fracture networks are considered and the effects on effective permeability discussed. In Section 4.2, it is shown that the Stokes-

Brinkman equations can naturally be used to model additional physical effects pertaining to vugular media such as partial fracture with fill-in by some material and/or fluids with suspended solid particles.

2 Mathematical models for Vuggy media at multiple scales

In this paper we consider a medium with two scales. The fine scale (e.g., the "meso-scale" in Fig. 1), whose characteristic length is denoted by l is composed of vugs, caves, fractures, and regular porous media. The vugs, caves and some of the fractures are mostly free-flow regions, while the porous part is characterized by Darcy flow. Note that the porous region, which we will also refer to as matrix, has a much finer underlying structure of impermeable solid and pore space where fluid flow occurs. This much finer structure (e.g., the "micro-scale" in Fig. 1) is not considered but an effective response of the porous media is assumed governed by material parameters such as porosity and permeability.

At the coarse scale (e.g., the "field-scale" in Fig. 1), whose characteristic length is denoted by L, the media is described mostly by Darcy flow. Fine scale features such as vugs, caves, and fractures, along with the surrounding porous matrix, are replaced by an effective material with well defined effective permeability and porosity. However, certain features, such as large, long-range caves (relative to the fine scale) may still be retained at the coarse scale. In the later situation, the Stokes-Brinkman model provides a natural way of transiting between the scales.

Based on the two characteristic length-scales l and L, the usual small parameter ε (c.f., e.g., [28, 32]) is introduced:

$$\varepsilon = \frac{l}{L}. \tag{2.1}$$

Throughout this paper, all quantities with subscript ε are defined on the fine scale, and quantities with superscript $*$ are defined on the coarse scale. At the fines scale, the free-flow domain (vugs, caves, fractures) is defined by Ω_ε^f and the porous part (effective media with certain permeability and porosity) by Ω_ε^p. Thus, the entire fine-scale domain Ω_ε is the union of the two disjoint domains Ω_ε^f and Ω_ε^p. The interface between the porous and free flow part (excluding the external boundary) is denoted by Γ_ε, that is, $\Gamma_\varepsilon = \partial\Omega_\varepsilon^f \cap \Omega_\varepsilon^p$. Next, the fine scale fluid velocity and pressure are denoted by $\mathbf{v}_\varepsilon$ and p_ε, respectively. In the free flow region, $\mathbf{v}_\varepsilon$ represents the actual physical velocity of the fluid but in the porous region Ω_ε^p it represents the Darcy (or averaged) velocity.

The two mathematical models for the fine scale: the Stokes-Darcy (Section 2.1) and the alternative proposed in this work, the Stokes-Brinkman model (Section 2.2), are presented next. This is followed by a short discussion on the upscaling of the Stokes-Brinkman equation from the fine to the coarse scale in Section 2.3.

2.1 The Darcy-Stokes model

The Stokes equation, used to describe the free flow region, has the form (c.f., e.g., [12,22]):

$$\nabla p_\varepsilon - \mu \Delta \mathbf{v}_\varepsilon = \mathbf{f} \qquad \text{in } \Omega_\varepsilon^f, \tag{2.2}$$

$$\nabla \cdot \mathbf{v}_\varepsilon = 0 \qquad \text{in } \Omega_\varepsilon^f. \tag{2.3}$$

The first of these equation expresses the balance of linear momentum and the second is the conservation of mass. Also, recall the fluid stress tensor σ_ε, given by the formula:

$$\sigma_\varepsilon = -p_\varepsilon \mathbf{I} + 2\mu \mathbf{D}_\varepsilon,$$

where $\mathbf{D}_\varepsilon$ is the strain rate:

$$\mathbf{D}_\varepsilon = \frac{1}{2}\left(\nabla \mathbf{v}_\varepsilon + \nabla \mathbf{v}_\varepsilon{}^T\right).$$

In the porous region, one has the classical Darcy law (c.f., e.g., [8,28]), along with conservation of mass:

$$\mathbf{v}_\varepsilon = -\frac{\mathbf{K}}{\mu}(\nabla p_\varepsilon - \mathbf{f}) \qquad \text{in } \Omega_\varepsilon^p, \tag{2.4}$$

$$\nabla \cdot \mathbf{v}_\varepsilon = 0 \qquad \text{in } \Omega_\varepsilon^p. \tag{2.5}$$

The two systems need to be coupled at the interface Γ. There are various ways in which this is achieved. For example, the classical condition of [4] states that:

$$[\mathbf{v}_\varepsilon] \cdot \mathbf{n} = 0 \qquad \text{on } \Gamma_\varepsilon, \tag{2.6}$$

$$2\mu \mathbf{D}_\varepsilon \mathbf{n} = [p_\varepsilon] \qquad \text{on } \Gamma_\varepsilon, \tag{2.7}$$

$$\frac{\partial \mathbf{v}_\varepsilon^f}{\partial \mathbf{n}} = -\frac{\alpha_{BJ}}{\sqrt{K}}[\mathbf{v}_\varepsilon] \cdot \mathbf{t}_i \qquad \text{on } \Gamma_\varepsilon. \tag{2.8}$$

Here, $[\cdot]$ denotes the jump in a given quantity while moving from the fluid to the porous side, that is, form some field ϕ:

$$[\phi] = \phi_f - \phi_p,$$

$\mathbf{n}$ is a unit normal pointing from Ω_ε^f to Ω_ε^p and $\mathbf{v}_\varepsilon^f$ is the velocity in the fluid region. In the above equations, the first interface condition (2.6) expresses conservation of mass across the interface, (2.7) expresses conservation of momentum, and (2.8) imposes a slip condition on the tangential component of the velocity. The dimensionless constant α_{BJ} is a material property which is representative of the microstructure (at much smaller scales than l) of the interface. It can be obtained either numerically, if such information is available, or obtained experimentally. The first approach is accessible to engineered media, where often the microstructure of the porous media is known. The second approach is more appropriate for natural media such as reservoir formations, where precise knowledge of the microstructure is very difficult, if not impossible to obtain.

It should be emphasized, that the exact form of the interface conditions (2.6)-(2.8) is an active area of research (c.f., e.g., [4, 14–16, 20, 26, 29]). For example, Saffman [26] modified equation (2.8) to contain only variables in the fluid domain, while others [20,29] studied the interface conditions based on the flow type, e.g., parallel or perpendicular to the interface [20, 29]. The mathematical justifications of such interface conditions can be found, for example in [14–16]. The reader is referred to [19] for a detailed review.

2.2 The Stokes-Brinkman model

Recall that the fine scale velocity is denoted by $\mathbf{v}_\varepsilon$ and the fine scale pressure by p_ε. The Stokes-Brinkman equation for a single phase flow in a porous/free flow media is written as follows (c.f., e.g., [5, 19]):

$$\mu\mathbf{K}^{-1}\mathbf{v}_\varepsilon+\nabla p_\varepsilon-\tilde{\mu}\Delta\mathbf{v}_\varepsilon=\mathbf{f} \qquad \text{in } \Omega_\varepsilon, \tag{2.9}$$

$$\nabla\cdot\mathbf{v}_\varepsilon=0 \qquad \text{in } \Omega_\varepsilon. \tag{2.10}$$

Here, $\mathbf{K}$ is a permeability tensor, which in Ω_ε^p is equal to the Darcy permeability of the porous media, μ is the physical viscosity of the fluid, and $\tilde{\mu}$ is an effective viscosity. $\mathbf{K}$ and $\tilde{\mu}$ are selected differently depending on the media type (porous or free flow) and are discussed next. Based on this selection, in the fluid region, $\mathbf{v}_\varepsilon$ represents the actual physical velocity of the fluid and in the porous region it is the Darcy velocity.

The physical fluid viscosity μ is a material constant that defines the fluid under consideration (e.g., water, oil, etc) and is a uniform constant in the entire domain Ω_ε. In the fluid region Ω_ε^f, $\mathbf{K}$ is taken to be ∞ and $\tilde{\mu}$ is taken equal to the physical fluid viscosity μ:

$$\tilde{\mu}=\mu, \qquad \mathbf{K}=\infty \qquad \text{in } \Omega_\varepsilon^f \tag{2.11}$$

Observe that this selection of parameters implies that Eqs. (2.9)-(2.10) reduce to the Stokes system (2.2)-(2.3).

In the porous region Ω_ε^p, $\mathbf{K}$ is taken to be the Darcy permeability of the porous media. With that, and in the absence of distributed body force $\mathbf{f}$, Eq. (2.9) can be written as

$$\nabla p_\varepsilon=-\mu\mathbf{K}^{-1}\mathbf{v}_\varepsilon+\tilde{\mu}\Delta\mathbf{v}_\varepsilon \qquad \text{in } \Omega_\varepsilon^p, \tag{2.12}$$

The reader will recognize that in the last equation, the only difference with Darcy's law (2.4) is the additional viscous term $\tilde{\mu}\Delta\mathbf{v}_\varepsilon$. So, if $\tilde{\mu}$ is taken equal to zero in Ω_ε^p, then Eq. (2.9) reduces to (2.4). However this will reduce the Stokes-Brinkman system to the coupled Darcy-Stokes model. This will entail the difficulties mentioned previously in Section 2.1, which we aim to avoid. Observe, that in most porous media, $\mathbf{K}$ is in the range of milli- to tens of Darcy. Thus, if $\tilde{\mu}$ is of the same order as the physical viscosity μ, that is,

$$\tilde{\mu}\sim\mu,$$

the term $\mu\mathbf{K}^{-1}\mathbf{v}_\varepsilon$ in Eq. (2.12) dominates by many orders of magnitude $\tilde{\mu}\Delta\mathbf{v}_\varepsilon$. Thus, the additional viscous term introduces only a small perturbation to Darcy's law. As a result the simplest possible choice for $\tilde{\mu}$ is

$$\tilde{\mu}=\mu,$$

which can be physically motivated using thermodynamics of continuum media along with mixture theories [25]. This is also a typical choice used by modelers when complex geometries with uncertain interface location and/or lack of knowledge of the micro-scale interface features is involved [19, p. 26-29]. A different choice of $\tilde{\mu}$ is usually motivated by two factors.

First, $\tilde{\mu}$ can be used to provide a more accurate model for the porous medium than is afforded by Darcy law [18,21,23]. The difference becomes important for high porosity mediums. Lundgren [21] has considered flow through a random, moderately dense bed of spheres and found a dependence

$$\tilde{\mu}=\mu/(1-2.6\phi),$$

where ϕ is the volume fraction of spheres. Other have used a dilute limit calculation and a self-consistent approximation [18], and found that values for $\tilde{\mu}$ are generally smaller than μ in Ω_ε^p. For example, Martys er al. [23] have studied randomly generated 3D porous geometries and used 3D numerical simulations to provide a fit for $\tilde{\mu}$ for porosities between 0.5 and 0.8.

The effective viscosity $\tilde{\mu}$ can also be used to mimic various jump condition at the interface. For example, Neale and Nader [24] have found that the relation

$$\sqrt{\tilde{\mu}/\mu}=\alpha_{BJ},$$

where α_{BJ} is the constant used in the Beavers-Joseph condition, introduces a boundary layer near the interface. The rapid change in the fluid velocity in this layer leads to an effective jump, similar to the one observed in Darcy-Stokes models with a Beavers-Joseph condition. These types of approaches however are not very practical for reservoir simulations, due to the difficulty in obtaining values for α_{BJ}. Moreover, based on direct numerical simulations, Sahraoui and Kaviany [27] have reported that the relation $\sqrt{\tilde{\mu}/\mu}=\alpha_{BJ}$ does not model well the flow inside the porous region at high porosities. Instead, they have proposed hybrid models with $\tilde{\mu}$ varying spatially near the interface to both capture the correct fluid behavior inside the porous region as well as to capture different jump conditions at the interface.

In conclusion, the Stokes-Brinkman equation offers several advantages. First, it allows a unified approach to the ensemble of porous and free-flow media by formulating a single equation in the entire domain Ω_ε. The different media types are distinguished by proper selection of $\mathbf{K}$ and $\tilde{\mu}$ in Eqs. (2.9)-(2.10) and there is no need to formulate specific interface conditions, as in the coupled Darcy-Stokes approach. This is especially helpful when the porous domain Ω_ε^p has a complicated topology, as is the case in vuggy reservoirs. The unified approach also translates to significant simplification in the numerical treatment of Eqs. (2.9)-(2.10).

2.3 Upscaling

As was mentioned earlier, vuggy, fractured reservoirs feature multiple scales, and upscaling is necessary for numerical simulation at the field scale (Fig. 1). In this section, we consider the upscaling of the Stokes-Brinkman equation from the fine to the coarse scale. The short summary presented next is based on two-scale asymptotic expansion (c.f., e.g., [28, 32]). The procedure is very similar to the one employed for upscaling the Stokes equation in an impermeable porous media. The reader is thus referred to [11] for technical details.

First, we assume that we have a Representative Element of Volume (REV) which features both porous and fluid domains. A formal asymptotic expansion of the type:

$$\mathbf{v}_\varepsilon(\mathbf{x}) = \mathbf{v}_{-2}(\mathbf{x},\mathbf{y}) + \varepsilon \mathbf{v}_{-1}(\mathbf{x},\mathbf{y}) + \varepsilon^2 \mathbf{v}_0(\mathbf{x},\mathbf{y}) + \varepsilon^3 \mathbf{v}_1(\mathbf{x},\mathbf{y}) + \cdots, \tag{2.13}$$

$$p_\varepsilon(\mathbf{x}) = p_0(\mathbf{x},\mathbf{y}) + \varepsilon p_1(\mathbf{x},\mathbf{y}) + \cdots \tag{2.14}$$

is substituted in Eqs. (2.9)-(2.10). By further assuming that

$$\mu \mathbf{K}^{-1} \geq \mathcal{O}\left(\varepsilon^{-2}\right), \tag{2.15}$$

one obtains that the first two velocity terms $\mathbf{v}_{-2}$ and $\mathbf{v}_{-1}$ are identically zero and the first term in the pressure expansion p_0 does not depend on the fine-scale variable $\mathbf{y}$, that is $p_0 = p_0(\mathbf{x})$.

Next, one obtains a set of cell problems that are used to compute the effective (or upscaled) permeability of the REV. Let d be the dimension (2 or 3) and $\mathbf{e}_i$ be a unit vector in the i-th direction. The d cell problems needed to upscale the Stokes-Brinkman equation are:

$$\mathbf{K}^{-1}\mathbf{w}^i + \nabla_{\mathbf{y}} q^i - \frac{\tilde{\mu}}{\mu}\Delta_{\mathbf{y}}\mathbf{w}^i = \mathbf{e}_i \qquad \text{in } Y, \tag{2.16}$$

$$\nabla_{\mathbf{y}} \cdot \mathbf{w} = 0 \qquad \text{in } Y. \tag{2.17}$$

Here, $\mathbf{w}^i$ are Y-periodic and the (fine-scale) pressure q has zero average in Y. The macroscopic (upscaled) permeability $\mathbf{K}^*$ is then computed by averaging the fine-scale velocities:

$$K^*_{ij} := \langle w_i{}^j \rangle_Y = \frac{1}{|Y|}\int_Y w_i{}^j d\mathbf{y}. \tag{2.18}$$

The macroscopic (upscaled) flux is given by the Darcy's law:

$$\langle \mathbf{v}_\varepsilon \rangle = -\frac{\mathbf{K}^*}{\mu}\left(\nabla \langle p_\varepsilon \rangle - \mathbf{f}\right), \tag{2.19}$$

and subject to conservation of mass:

$$\nabla \cdot \langle \mathbf{v}_\varepsilon \rangle = 0, \tag{2.20}$$

Note that $\mathbf{w}^i$, $i=1,\cdots,d$ are the fine-scale velocities in the REV, that is Y, are subject to unit forcing in the respective direction. Since $\mathbf{e}_i$ can also be transferred to the pressure term:

$$\nabla\left(\mathbf{q}^i+x_i\right)=\nabla\mathbf{q}^i+\mathbf{e}_i,$$

one can consider $\langle\mathbf{w}^i\rangle$ as the averaged flux in Y over a unit pressure drop in the i-th coordinate direction.

The above upscaling works well under the assumption (2.15) and that an REV consisting of both porous and fluid region exists. Assumption (2.15) is quite general, since typically $\mathbf{K}^{-1}$ dominates the fluid viscosity by orders of magnitude. When $\mathbf{K}\sim\varepsilon^2\mu$ the Brinkman term in the porous part of Eq. (2.16) is significant. The fine-scale velocities in the porous and fluid region will be of similar orders and noticeable mass transfer will occur between the fluid and solid, regardless of the flow regime. When $\mathbf{K}\ll\varepsilon^2\mu$, the Brinkman term in (2.16) will dominate in the porous part of Y. As a result, the flow will significantly depend on the geometry of the REV. For example, in the case of connected vugs, the flow trough the vugs will dominate any flow in the porous part and one will essentially be homogenizing Stokes flow in impermeable media.

It is also possible that the some regions of the fine-scale domain does not allow upscaling, for example when an REV contains only a fluid domain. This will happen if there are fluid regions with characteristic size much larger then l, c.f., Eq. (2.1). In such cases one can upscale the part of the fine scale where suitable mixture of porous media and vugs exist. Large scale voids on the other hand can be retained as free flow regions at the coarse scale. Then one will have a homogenized Stokes-Brinkman equation of the type:

$$\mu(\mathbf{K}^*)^{-1}\mathbf{v}^*+\nabla p^*-\tilde{\mu}\Delta\mathbf{v}^*=\mathbf{f} \qquad \text{in } \Omega^*, \tag{2.21}$$

$$\nabla\cdot\mathbf{v}^*=0 \qquad \text{in } \Omega^*. \tag{2.22}$$

where the fluid region is represented by vugs, caves or fractures that cannot be homogenize. The porous region is the part susceptible to homogenization. There, the macroscopic (coarse-scale) velocity $\mathbf{v}^*$ and pressure p^* are defined as the average of the respective fine-scale quantities:

$$\mathbf{v}^*=\langle\mathbf{v}_\varepsilon\rangle, \quad p^*=\langle p_\varepsilon\rangle \tag{2.23}$$

and the coarse-scale velocity $\mathbf{v}^*$ is connected to the pressure gradient ∇p and the distributed forcing by Eq. (2.19). The permeability $\mathbf{K}^*$ is obtained using Eq. (2.18) and the cell problems (2.16)-(2.17). In the fluid region, $\mathbf{v}^*$ is again the actual physical velocity.

In this way, the Stokes-Brinkman model makes it possible to upscale fractured, vuggy media, in a natural way, in a sense that the same equation is retained at all scales. This allows successive homogenization at multiple scales such as the one shown in Fig. 1.

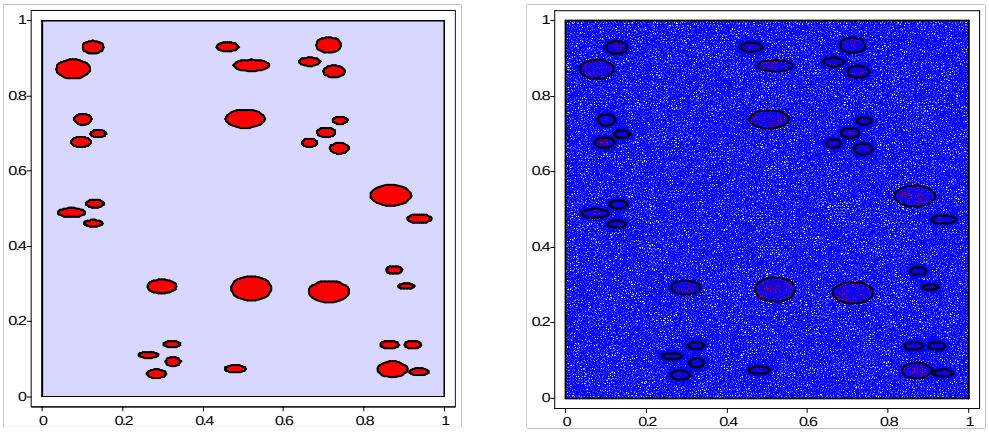

(a) Fine-scale domain (b) Fine-scale discretization

Figure 2: Fine scale domain (a) consisting of porous rock and randomly distributed elliptical vugs (red). The unstructured mesh used in computing the fine-scale solution is shown to the right (b).

3 Upscaling of porous media with randomly distributed, disconnected vugs

In this section we perform two numerical simulations designed to test the upscaling of the Stoke-Brinkman equations. Both problems are set on the fine-scale domain shown in Fig. 2(a). The domain consists of matrix (e.g., porous rock) populated with randomly distributed ellipsoidal vugs. The vugs are completely free-flow regions, e.g., $K=\infty$ inside the vugs. The relatively simple shape of the vugs and the fact that they are not connected, allows us to investigate the upscaled behavior of the media and quantify the influence of the vugs. This is done by comparing numerically computed fine-scale flow fields for Eqs. (2.9), (2.10) with corresponding coarse scale fields obtained by upscaling the matrix/vug mixture to the Darcy model (2.19)-(2.20).

In all examples, the flow is driven from left to right by a pressure drop of $1Pa$ over the horizontal direction. That is, the pressure is set to $1Pa$ at the left side of the domain and zero at the right side. At the top and bottom sides no-flow boundary conditions are specified. The fluid under consideration is water ($\mu=1cP$). In the first example (Section 3.2) a constant matrix permeability is used, while in the second a variable matrix permeability is considered (Section 3.3).

3.1 Discretization

For both examples we compute a reference fine-scale solution, using the regular triangular mesh shown in Fig. 2(b). The mesh has 35272 elements of average diameter h=0.01. In order to solve numerically the fine-scale problem (2.9)-(2.10), as well as the cell problems (2.16)-(2.17) we use a mixed finite element method for the Stokes-Brinkman equations

in the primary variables. We use Taylor-Hood elements (continuous quadratic velocity and continuous linear pressure, for more details, see, e.g., [30]) on unstructured grids. The Taylor-Hood element is one of the few commonly used elements for the Stokes equation which is also stable for the Stokes-Brinkman equation [6]. It also provides a good approximation for both velocity and pressure.

The linear systems resulting from this finite element discretization are symmetric and indefinite and are solved using preconditioned conjugate gradient method for the pressure Schur complement. For more details on these types of numerical the reader is referred to [30]. The coarse-scale problems (2.19)-(2.20) are solved by standard, conforming finite element method (c.f., e.g., [7]).

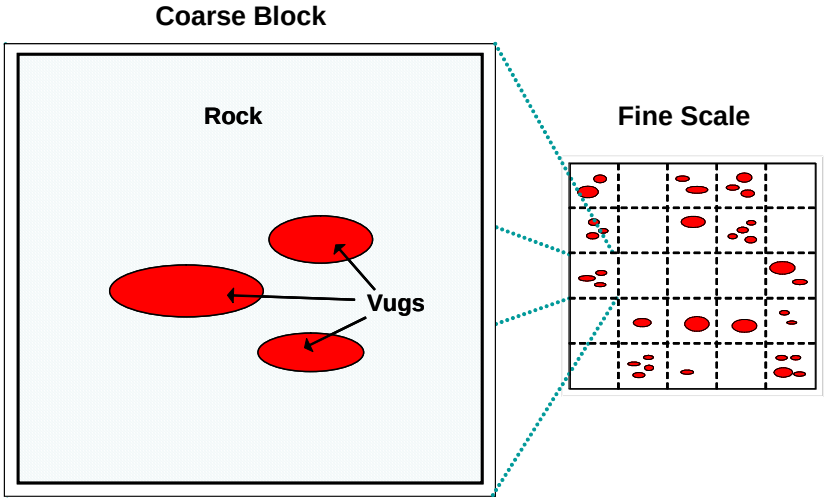

Figure 3: Coarse block partitioning of the fine-scale domain.

The upscaling, again in both cases, is performed as follows. The whole domain is divided into 5×5 coarse grid blocks, as shown in Fig. 3. For each coarse grid, the upscaled permeability $\mathbf{K}^*$ is computed (c.f., the cell problems (2.16)-(2.17)) and the averaging equation (2.18). The resulting Darcy equation (2.19)-(2.20) is solved by standard linear finite elements and a coarse scale pressure is obtained.

Before presenting the results in details, let us note that the there were no free flow regions at the coarse scale, therefore, one could use a conforming method for the coarse scale diffusion equation (e.g., Eqs. (2.19)-(2.20)). This was done purely for convenience as our main goal was to demonstrate the applicability of upscaling vuggy media, modeled by the Stokes-Brinkman equation at the fine-scale. Note that in a multiphase flow and transport simulation of realistic reservoirs one should use a mixed method or other mass conservative methods at the coarse scale because mass conservative velocity field is needed for solving the transport equation. This should also be done when the coarse-scale equation is again Stokes-Brinkman model (c.f., Eqs. (2.21), (2.22)), for example due to larger vugs that cannot will be visible across scales (Fig. 1).

3.2 Homogeneous matrix permeability

In the first example, the background permeability field is homogeneous with $K = 1mD$. The fine-scale solution is shown in Fig. 4. It can be seen that, the velocity inside the vugs several times bigger than in the matrix and connected nearby vugs tend to create flow-channels. Moreover, the velocity profile in elongated vugs resembles that of a Poiseuille flow with the maximum velocity in the center of the vug.

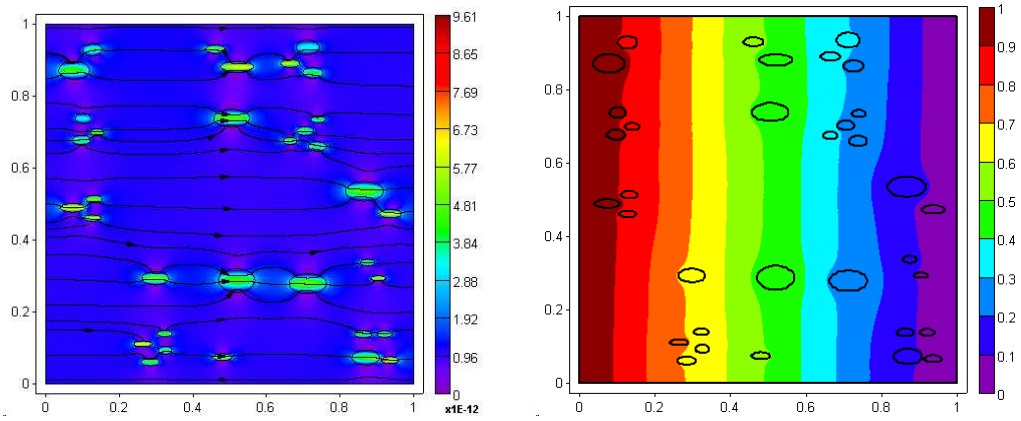

(a) Streamlines and velocity magnitude (b) Pressure field

Figure 4: Fine scale reference solution (homogeneous matrix permeability).

Next, the whole domain is divided into 5×5 coarse grid blocks (Fig. 3). For each coarse grid, the upscaled permeability $\mathbf{K}^*$ is computed (c.f., the cell problems (2.16)-(2.17)) and the averaging equation (2.18). The horizontal and vertical components K^*_{11} and K^*_{22} of the upscaled permeability tensor $\mathbf{K}^*$ are shown in Fig. 5. We observe from this figure that in the coarse regions with high concentration of vugs, the upscaled permeability is higher. The upscaled permeability is approximately 30-50% higher than the matrix permeability.

In Fig. 6(a), we plot the corresponding coarse-scale pressure. Since the difference with the fine-scale pressure (Fig. 4(b)) is difficult to discern, we have subtracted $1-x$ (the pressure drop) from both the coarse- and fine-scale pressure fields and plotted the results in Figs. 6(b) and 6(c), respectively. Furthermore, we have compared this coarse-scale pressure with the averaged coarse-scale pressure obtained from fine-scale solution. The relative L_2 error is found to be less than 2%. This result suggests that the proposed upscaling method provides accurate coarse-scale solution for homogeneous background permeability field.

3.3 Variable matrix permeability

In this example we replace the homogeneous matrix with a heterogeneous, isotropic matrix permeability, as shown in Fig. 3.3. This more realistic example allows us to investigate

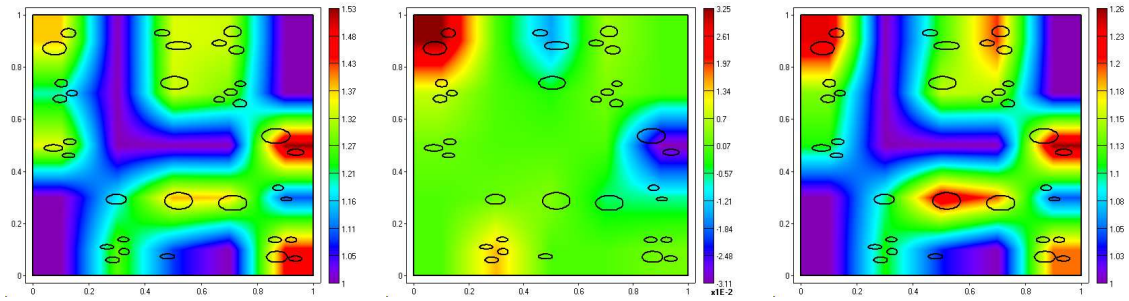

(a) K_{11} (b) K_{12} (c) K_{22}

Figure 5: Upscaled permeability (in mD) for constant rock permeability.

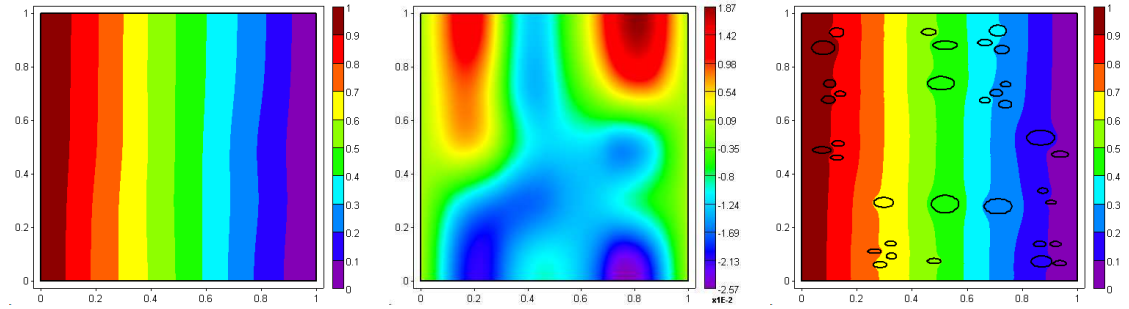

(a) Coarse-scale pressure p^*. (b) Variation in coarse-scale pressure (plotted is $p^*-(1-x)$). (c) Variation in fine-scale pressure (plotted is $p_\varepsilon-(1-x)$).

Figure 6: Homogeneous matrix. Comparison between the coarse-scale pressure (a) and reference solutions. In order to emphasize the difference between the two, the variation in the pressure (by subtracting the linear drop $1-x$) is plotted in (b) and (c).

the interplay between the vugs and the high-permeability channels which are present in the matrix permeability.

The vug population (size, shape and locations) are identical to the previous example (Fig. 2(a)). The fine-scale matrix permeability field is a realization of a stochastic field with prescribed overall variance (quantified via σ^2, the variance of $\log(k)$), correlation structure and covariance model. It was generated using the GSLIB algorithms [9], characterized by a spherical variogram. The field has long correlation length in the horizontal direction (0.4) and smaller correlation length in the vertical direction (0.1). The permeability field has an average of $1mD$ and range of the values is three orders of magnitude.

In Fig. 8, the fine-scale solution is plotted for velocity and pressure fields. We see from this figure that the heterogeneous permeability field creates additional high flow channels for the vugs which can enhance connectivity of the media. This is more evident if one compares Figs. 4 and 8. The presence of heterogeneous matrix permeability field also alters the velocity streamlines significantly.

The upscaling was performed on the same 5×5 coarse grid (Fig. 3), as in the previous

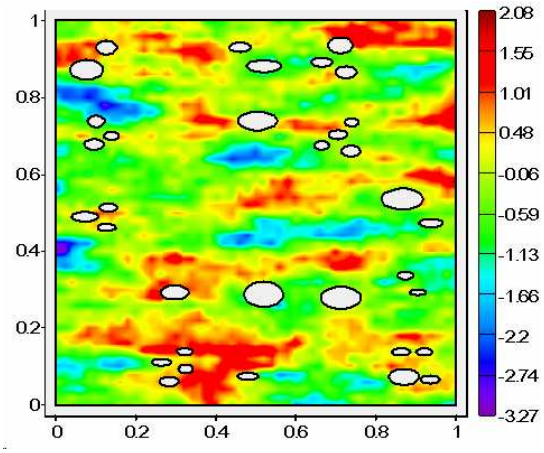

Figure 7: Log plot of the permeability field. The actual permeability used is $k = C\exp(\cdot)$, where C is selected so that the average of k is $1mD$.

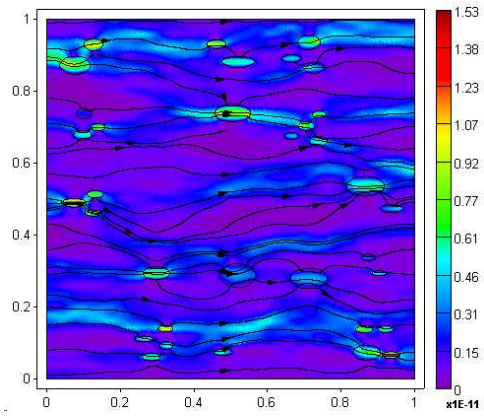

(a) Streamlines and velocity magnitude.

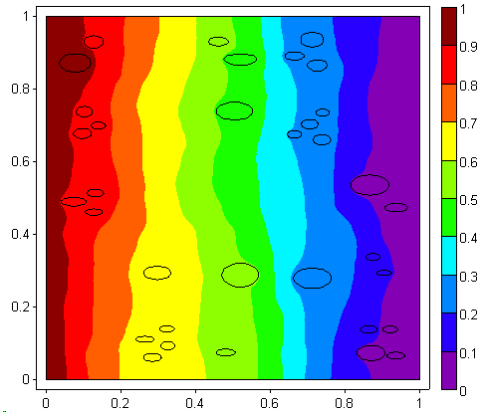

(b) Variation in the pressure (plotted is $p-(1-x)$).

Figure 8: Fine scale reference solution (heterogeneous matrix permeability).

example. Comparing Fig. 6 and Fig. 10, one can also observe that the upscaled permeability fields $\mathbf{K}^*$ are quite different for homogeneous and heterogeneous background permeabilities. The highest permeability in the case of heterogeneous background permeability is $3.36mD$, while the highest permeability in the case of homogeneous background permeability is only $1.53mD$. Moreover, one can also observe different pattern structure in the plots of upscaled permeabilities.

Based on the computed upscaled permeability field $\mathbf{K}^*$, the Darcy model was again solved and the upscaled pressure obtained (Fig. 10(a)). By comparing the upscaled pressure with the averaged fine-scale pressure it is found that the relative L_2 error is less than 5%. This result again suggests that the proposed upscaling method provides accurate coarse-scale solution for heterogeneous background permeability field.

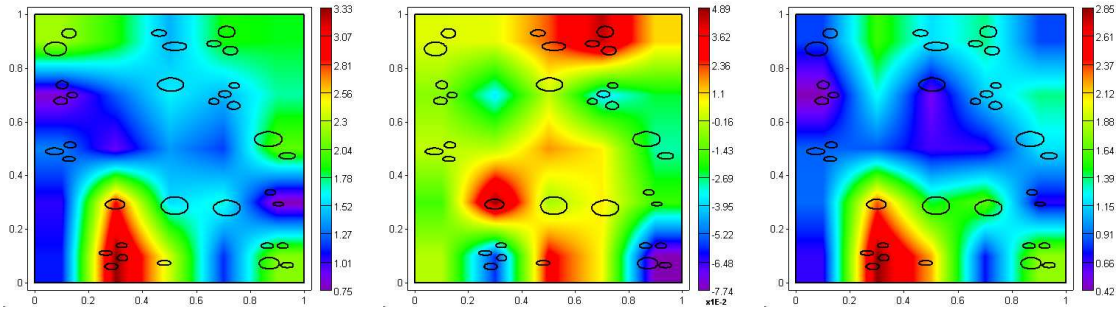

(a) K_{11} (b) K_{12} (c) K_{22}

Figure 9: Upscaled permeability (in mD).

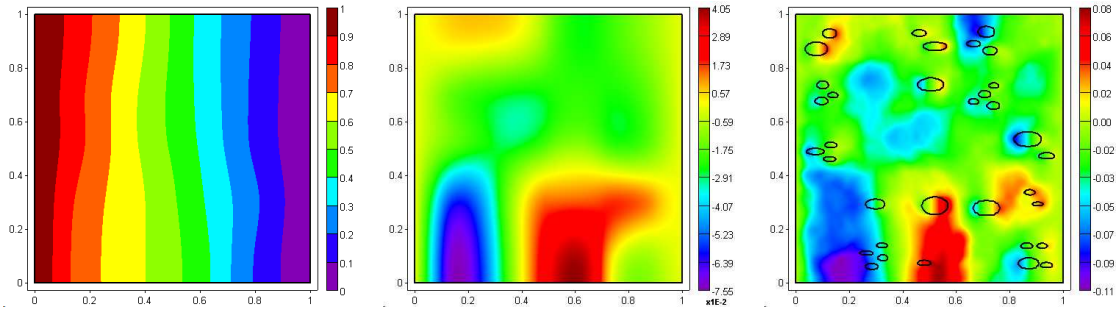

(a) Coarse-scale pressure p^*. (b) Variation in coarse-scale pressure (plotted is $p^*-(1-x)$). (c) Variation in fine-scale pressure (plotted is $p_\varepsilon-(1-x)$).

Figure 10: Heterogeneous matrix. Comparison between the coarse-scale pressure (a) and reference solutions. In order to emphasize the difference between the two, the variation in the pressure (by subtracting the linear drop $1-x$) is plotted in (b) and (c).

4 Modeling of vugs connected by fracture networks

In addition to vugs/caves, karst reservoirs typically also feature a variety of fractures. These can be long-range fractures (hundreds of meters scale), short range fractures (meters scale) and micro-fractures, at millimeter scale. A realistic reservoir can have very complex fracture/vug topology with some vugs being connected by fractures of different physical characteristics (aperture, roughness, fill-in material) while other vugs may be isolated and surrounded only by porous rock.

In this section we study the interaction between fractions, vugs and the porous matrix. We first take several representative coarse blocks which include different combinations of vugs and fractures and we compute their effective permeability (Section 4.1). We also demonstrate how the Stokes-Brinkman equation can be used to model fractures, caves and vugs which are partially filled with material such as sand, gravel, mud, etc (Section 4.2).

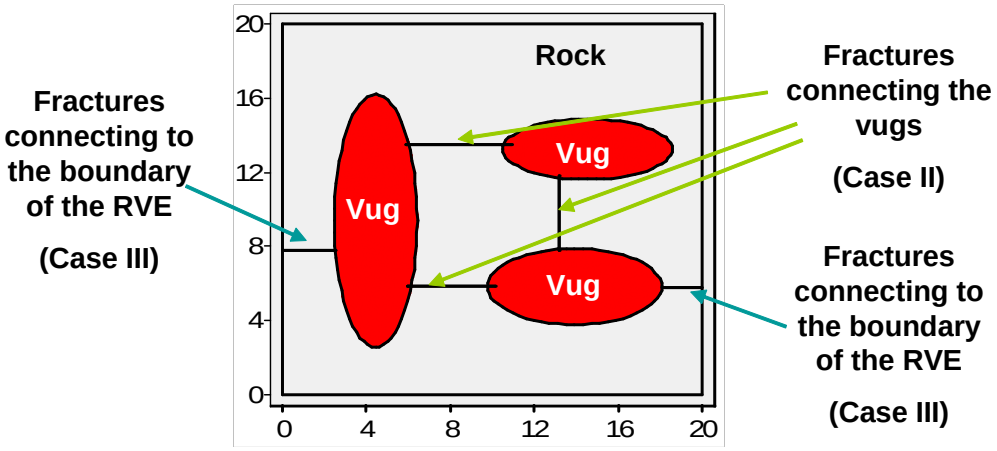

Figure 11: Vugs interconnected by a fracture network.

4.1 Effects of vugs connected by fractures

Here we evaluate the effective permeability of a model REV with vugs, interconnected by a fracture network. The coarse block contains three large elliptical vugs imbedded inside the porous matrix, as shown in Fig. 11. A fracture network connecting the vugs as well as the boundary of the REV was also established. Three cases were considered:

- *Case I*: The effective permeability tensor $\mathbf{K}^*$ for the entire block was computed ignoring all the fractures (Fig. 12(a)). That is, the fractures are considered part of the porous matrix.
- *Case II*: The three fractures connecting the vugs were included in the computation, but the two cracks connecting the vugs to the boundary of the REV were not included (Fig. 12(b)), that is, they were considered part of the porous matrix. This simulation is representative of a (part) of reservoir where only short-range fractures are present, that is, one can select an REV, representative of the vug population, which completely contains the fractures.
- *Case III*: All the fractures were included in the simulation (Fig. 12(c)). This simulation is relevant to (parts) of reservoirs with long-range fractures, that is, any REV, representative of the vug population, is much smaller than the characteristic length of the fractures.

The first case is similar to the computations performed previously in Section 3. It serves as a baseline against which the presence of fractures, both short- and long-range (*Cases II* and *III*, respectively), can be assessed quantitatively.

The simulations are set-up as follows: We use the Stokes-Brinkman model (2.9)-(2.10). The coarse block has dimensions $20\times 20m$. The porous matrix has a uniform permeability of $\mathbf{K}_r = 1mD$. The fractures are straight and have aperture in the range 1.1–1.7cm. They

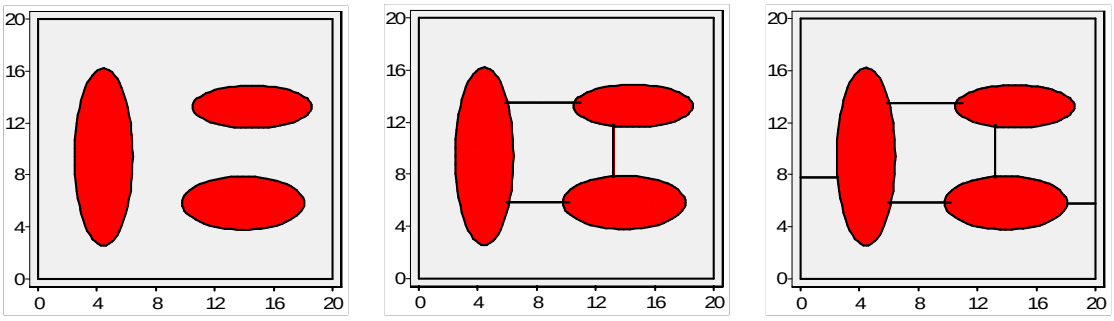

(a) *Case I*: Disconnected vugs.

(b) *Case II*: Short range fractures connecting the vugs.

(c) *Case III*: Short and long range fractures running through the vugs and REV.

Figure 12: Representative cases of vugs and fracture networks.

also are assumed to have completely smooth surface. When a fracture is included in the simulation, it is treated as a free flow region ($K_f = \infty$). When a fracture is not included in a simulation it is assigned the same permeability as the surrounding rock matrix ($K_f = \mathbf{K}_r$). The effective permeability of the block is computed by solving the cell problems (2.16)-(2.17).

The results of the simulations are presented in Table 1. As expected, *Case I* is similar to the upscaling calculations of the precious section. The upscaled permeability $\mathbf{K}^*$ increased about 70%–90% compared to the background matrix permeability ($\mathbf{K}_r$).

Table 1: Effective permeabilities for a coarse block with vugs connected by a fracture network.

	Case I	Case II	Case III
Effective REV Permeability $\mathbf{K}^*$ (in mD)	$\begin{pmatrix} 1.72 & 0.0 \\ 0.0 & 1.92 \end{pmatrix}$	$\begin{pmatrix} 3.35 & 0.0 \\ 0.0 & 2.37 \end{pmatrix}$	$\begin{pmatrix} 13.2 & -1.35 \\ -1.35 & 0.14 \end{pmatrix} \times 10^6$

The calculation of *Case II* show that connecting the vugs by short-range fractures of centimeter size nearly doubled the effective permeability in the horizontal direction in comparison to the basic *Case I*. The vertical permeability grew by another 20%. The larger increase in horizontal permeability is probably due to the fact that two of the three fractures run in that direction. Also, while having big effect, $\mathbf{K}^*$ remained in the same milli-Darcy range as the background matrix permeability ($\mathbf{K}_r = 1mD$). This can be easily explained by realizing that the fluid cannot enter the vugs directly but needs to pass through the matrix, thus the matrix determines the order of magnitude of the overall permeability.

The results for *Case III* show permeability about six to seven orders of magnitude larger than the matrix permeability. This implies that most of the flow runs directly trough the fractures and the matrix contributes very little to the overall flow rate. This result can be compared to the analytical results for permeability of a straight, smooth

fracture running trough an impermeable block. Using the classical formula [3]:

$$k=\frac{h^3}{12L},$$

where h is the aperture of the fracture and L the length of the block, one sees, that a $1cm$ straight, smooth fracture running trough a $20m$ block (without any vugs) will lead to effective permeability of $4.17\times10^6 mD$ which is in the same range. Note also that the off-diagonal components are non-zero. This is due to the fact the REV is not completely symmetric.

The results of *Case III* raise two important questions. First, how to upscale REVs in the presence of long range fractures. And, secondly, what other physical effects become important in such situations.

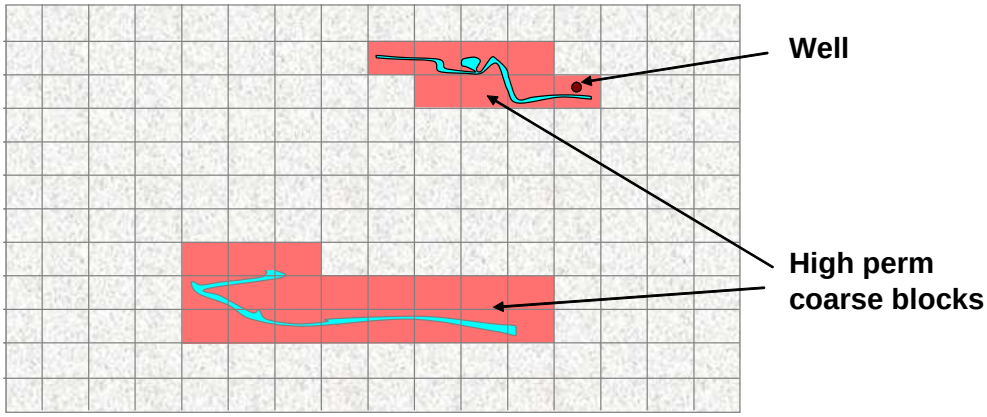

Figure 13: A coarse scale discretization of a long-range fracture.

The upscaling of REVs with long-range fractures should be considered in the context of the coarse scale problem. Suppose for example, that such coarse blocks occur away from injection or production wells. Then a coarse scale discretization can easily cover an entire long-range fracture with several coarse scale blocks. While each of these blocks will have very high permeability, they will be surrounded by low-perm blocks as shown in Fig. 13. Thus, in the absence of any direct link to high flow rate sources such as a well, such a coarse scale discretization will capture correctly the macroscopic solution. If however there are large flow rate sources nearby the fracture, then direct upscaling will likely lead to poor results. In such situations it will be necessary to consider near well models in conjunction with an iterative homogenization technique (c.f., e.g., [10,31]).

4.2 Modeling of fracture fill-in

The simulations for *Case III* of Section 4.1 demonstrated the large impact a long-range fracture can have on the effective properties of a coarse block. However, in that simula-

tion, several physical aspects of fractures in karst reservoirs were not considered. First, fractures are never straight lines, but instead have complex shape. Moreover, fracture aperture is not constant, but can vary along the length of the fracture. In places a fracture may nearly close, due to local roughness of its surface. Secondly, the fracture itself need not be a completely free-flow area, but instead may have various types of filling, such as mud, sand, gravel, etc. All of these factors may alter the flow rate trough a fracture by orders of magnitude. Additionally, the fluid itself may have significant amount of suspended solid particles, which may alter the flow in a fracture.

In this section we address the problem of modeling fracture fill-in, as well as fluids with suspended rigid particles by means of the Stokes-Brinkman model (2.9), (2.10). As was mentioned earlier, the permeability of a free flow region is set to ∞ (c.f., Eq. (2.11)). However, in the case of fracture fill-in (partial or full) one may assign a finite permeability of the fracture. Depending on the type of the fill-in, the flow in the fracture may resemble Stokes flow (high porosity fill-in) or Darcy flow (low porosity fill-in). Thus, if the permeability of the fill-in material is known one may assign a finite permeability in the fracture and perform the scale-up. Such an approach can also be used if the fluid has suspended rigid particles.

To investigate the effects of finite permeability in a filled fracture, we performed a number of numerical simulation. The geometry under consideration was that of *Case III* of the previous section (Fig. 12(c)). The basic matrix permeability was taken to be $\mathbf{K}_r = 1D$. The permeability of the fractures K_f (all five of them) were assigned several different scalar permeabilities, ranging from the matrix permeability $1D$ to ∞. The vugs were always maintained free flow regions, that is, the permeability there was ∞.

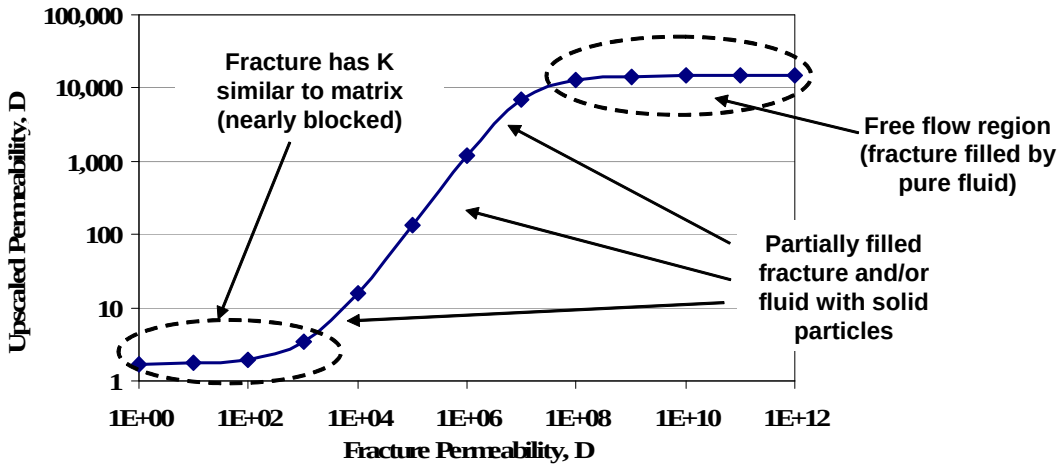

Figure 14: Effective permeability (K^*_{11} component) of the coarse block as a function of the fracture permeability.

The effective permeability $\mathbf{K}^*$ of the entire block was computed for each value of K_f. The results are shown in Fig. 14. At the bottom-left corner of the graph, the fracture

permeability K_f is equal to that of the matrix, that is the fractures are completely blocked. It can be seen that K_f needs to increase by a factor of 100, before a significant change in $\mathbf{K}^*$ occurs. The region in the right part of the graph on the other hand, is the free, or nearly free flow region. This flow regime starts at around $K_f \sim 10^8$–$10^9 D$ and an increase in K_f past that range does not visibly change $\mathbf{K}^*$. There is a large (six orders of magnitude), intermediate range of values of K_f (10^2–$10^8 D$), where the effective permeability changes smoothly form the low perm limit (blocked fracture) to the high perm limit (unobstructed fracture). Observe also that the change in $\mathbf{K}^*$ from blocked to unobstructed fracture is many orders of magnitude. Therefore, determining the presence and nature of the fill in material is an important part of a robust reservoir model.

As a concluding remark, note also, that the low permeability limit is dictated by the matrix, while the unobstructed fracture limit is controlled by the fracture network. Thus, a change in the fracture aperture in some of the fractures will change the high permeability limit, but will leave the low-permeability limit unchanged. Conversely, a change in the background matrix permeability will alter only the left part of the graph, but the high-permeability limit will remain unchanged as it is controlled by the fractures.

5 Conclusions

In this paper we have considered the Stokes-Brinkman equation as a fine-scale model for flows in vuggy, fractured karst reservoirs. We used a mixed finite element method to solve a number the fine-scale flow problems. We have analyzed both isolated vugs in porous matrix as well as vugs connected by fracture networks. It was proposed to use the Stokes-Brinkman equations to model fractures with fill in material and/or fluids with suspended solid particles.

The results of Section 3 show that a fine-scale model based on Stokes-Brinkman equation can be used to describe the flow through vugular porous media. We have performed upscaling of isolated vug population embedded in two different porous matrices by computing coarse-scale permeabilities as well as coarse scale flow fields. The numerical tests show that the proposed upscaling to Darcy law at the coarse scale is accurate in the case of isolated vugs. Our upscaled results also demonstrate that a heterogeneous background permeability field can give very different results compared to homogeneous background permeability with the same vug locations. The mechanism behind this is that vugs can connect otherwise disconnected high-perm regions in the rock matrix. This leads to the creation of high permeability channels of interconnected high-perm matrix regions and vugs, leading to substantial increase the overall permeability.

The interplay between vugs and fracture networks (Section 4) showed that two major cases exist — that of short and long-range fractures. The results demonstrate that the presence of a short-range fracture network connecting large vugs can change the effective permeability of a coarse block by a factor of 2-4. However, the effective permeability remains of the same order of magnitude and upscaling such media poses no challenges.

On the other hand, long range, large aperture, fractures, may change the effective permeability by many orders of magnitude. In such cases secondary effects, such as fracture fill-in and roughness become important and need to be included in the fine-scale simulations. If the fractures are unobstructed and the resulting effective permeability is very high it may be necessary to consider more complex coarse-scale models which involve near well modeling and/or iterative homogenization as done by [10, 31].

It was also shown (Section 4.2), that the Stokes-Brinkman equations allow the simulation of high porosity, but finite permeability fill-in regions in fractures and caves in a natural way. This feature of the Stokes-Brinkman model can be extended to also capture uncertainty in the interface location, damage zones near the interface and particle suspension in the working fluid.

Observe also that the present work can easily be extended to three spatial dimensions. The analysis in Section 2.3 is valid in both two and three spatial dimensions. Qualitatively, one can expect similar difference between connected vugs and disconnected ones. Parametrization based on the fracture fill-in material as done in Section 4.2 are again possible, however detailed knowledge of the three-dimensional fracture structure will be required to achieve meaningful results.

Acknowledgments

The authors would like to thank the China Petroleum & Chemical Corporation (SINOPEC), for supporting this work. We are also grateful for the fruitful discussions with Dr. Yang Li, Dr. Xiangchun Yuan and Dr. Jianglong Li during the course of this work.

References

[1] G. Allaire. Homogenization of the Navier-Stokes equations and derivation of Brinkman's law. In Mathématiques appliquées aux sciences de l'ingénieur (Santiago, 1989), pages 7–20. Cépaduès, Toulouse, 1991.
[2] T. Arbogast and H. L. Lehr. Homogenization of a Darcy-Stokes system modeling vuggy porous media. Comput. Geosci., 10(3):291–302, 2006.
[3] J. Bear. Dynamics of Fluids in Porous Media. Dover, New York, 1972.
[4] G.S. Beavers and D.D. Joseph. Boundary conditions at a naturally permeable wall. J. Fluid Mech., 30:197–207, 1967.
[5] H. C. Brinkman. A calculation of the viscous force exerted by a flowing fluid on a dense swarm of particles. Appl. Sci. Res. Sect. A-Mech. Heat Chem. Eng. Math. Methods, 1:27–34, 1947.
[6] E. Burman and P. Hansbo. A unified stabilized method for Stokes' and Darcy's equations. J. Comput. Appl. Math., 198:35–51, 2007.
[7] P. Ciarlet. The Finite Element Method for Elliptic Problems. Number 40 in Classics in Applied Mathematics. SIAM, Philadelphia, 2002.
[8] H. Darcy. Les fontaines publique de la ville de Dijon. Librairie des Corps Impériaux des Ponts et Chaussées et des Mines, Paris, 1856.

[9] C.V. Deutsch and A. G. Journel. GSLIB: Geostatistical Software Library and User Guide. New York, 2 edition, 1998.
[10] Y. Efendiev and A. Pankov. Numerical homogenization of monotone elliptic operators. Multiscale Model. Simulat., 2(1):62–79, 2003.
[11] H.I. Ene. Application of the homogenization method to transport in porous media. In J.H. Cushman, editor, Dynamics of Fluids in Hierarchical Porous Media, pages 223–241. Academic Press, London, 1990.
[12] M. E. Gurtin. An Introduction to Continuum Mechanics. Academics Press, San Diego, CA, 1981.
[13] U. Hornung. Homogenization and Porous Media. Interdisciplinary Applied Mathematics. 6. New York, Springer, 1997.
[14] W. Jaeger, A. Mikelic, and N. Neuss. Asymptotic analysis of the laminar viscous flow over a porous bed. SIAM J. Sci. Comput., 22(6):2006–2028, 2001.
[15] W. Jäger and A. Mikelić. On the boundary conditions at the contact interface between a porous medium and a free fluid. Ann. Scuola Norm. Sup. Pisa Cl. Sci. (4), 23(3):403–465, 1996.
[16] W. Jäger and A. Mikelić. On the interface boundary condition of Beavers, Joseph, and Saffman. SIAM J. Appl. Math., 60(4):1111–1127 (electronic), 2000.
[17] M. Kaviany. Principles of Heat Transfer in Porous Media. Mechanical Engineering Series. Springer-Verlag, New York, 1999.
[18] J. Koplik, H. Levine, and A. Zee. Viscosity renormalization in the Brinkman equation. Phys. Fluids, 26:2864–2870, oct 1983.
[19] V. Laptev. Numerical solution of coupled flow in plain and porous media. Ph.D. thesis, Technical University of Kaiserslautern, Germany, 2003.
[20] T. Levy and E. Sánchez-Palencia. On boundary conditions for fluid flow in porous media. Int. J. Engrg. Sci., 13(11):923–940, 1975.
[21] T. S. Lundgren. Slow flow through stationary random beds and suspensions of spheres. J. Fluid Mech., 51:273–299, 1972.
[22] L. E. Malvern. Introduction to the Mechanics of a Continuous Medium. Prentice-Hall, Inc., Englewood Cliffs, NJ, 1969.
[23] N. Martys, D. P. Bentz, and E. J. Garboczi. Computer simulation study of the effective viscosity in Brinkman's equation. Phys. Fluids, 6:1434–1439, apr 1994.
[24] G. Neale and W. Nader. Practical significance of brinkmans extension of darcys law - coupled parallel flows within a channel and a bounding porous-medium. Canadian J. Chem. Eng., 52:475–478, 1974.
[25] K.R. Rajagopal. On a hierarchy of approximate models for flows of incompressible fluids through porous solids. Math. Models Methods Appl. Sci., 17(2):215–252, 2007.
[26] P.G. Saffman. On the boundary condition at the surface of a porous medium. Studies Appl. Math., 50:93–101, 1971.
[27] M. Sahraoui and M. Kaviany. Slip and no-slip velocity boundary conditions at interface of porous, plain media. Int. J. Heat Mass Transfer, 35:927–943, 1992.
[28] E. Sanchez-Palencia. Non-Homogeneous Media and Vibration Theory, volume 127 of Lecture Notes in Physics. Springer-Verlag, Berlin, 1980.
[29] E. Sanchez-Palencia and H.I. Ene. Equations et phénomènes de surface pour l'écoulement dans un modèle de milieu poreux. Journal de Mécanique, 14:73–108, 1975.
[30] S. Turek. Efficient Solvers for Incompressible Flow Problems: An Algorithmic and Computational Approach. Springer Verlag, New York, 1999.

[31] X. H. Wu, Y. Efendiev, and L. Durlofsky. Analysis of upscaling absolute permeability. Discrete Contin. Dyn. Syst., Ser. B, 2(2):185–204, 2002.
[32] V.V Zhikov, S.M. Kozlov, and O.A. Oleinik. Homogenization of Differential Operators and Integral Functionals. Springer-Verlag, Berlin, 1994.